iScience

CellPress
OPEN ACCESS

Article

Myeloid-cell-specific role of Gasdermin D in promoting lung cancer progression in mice

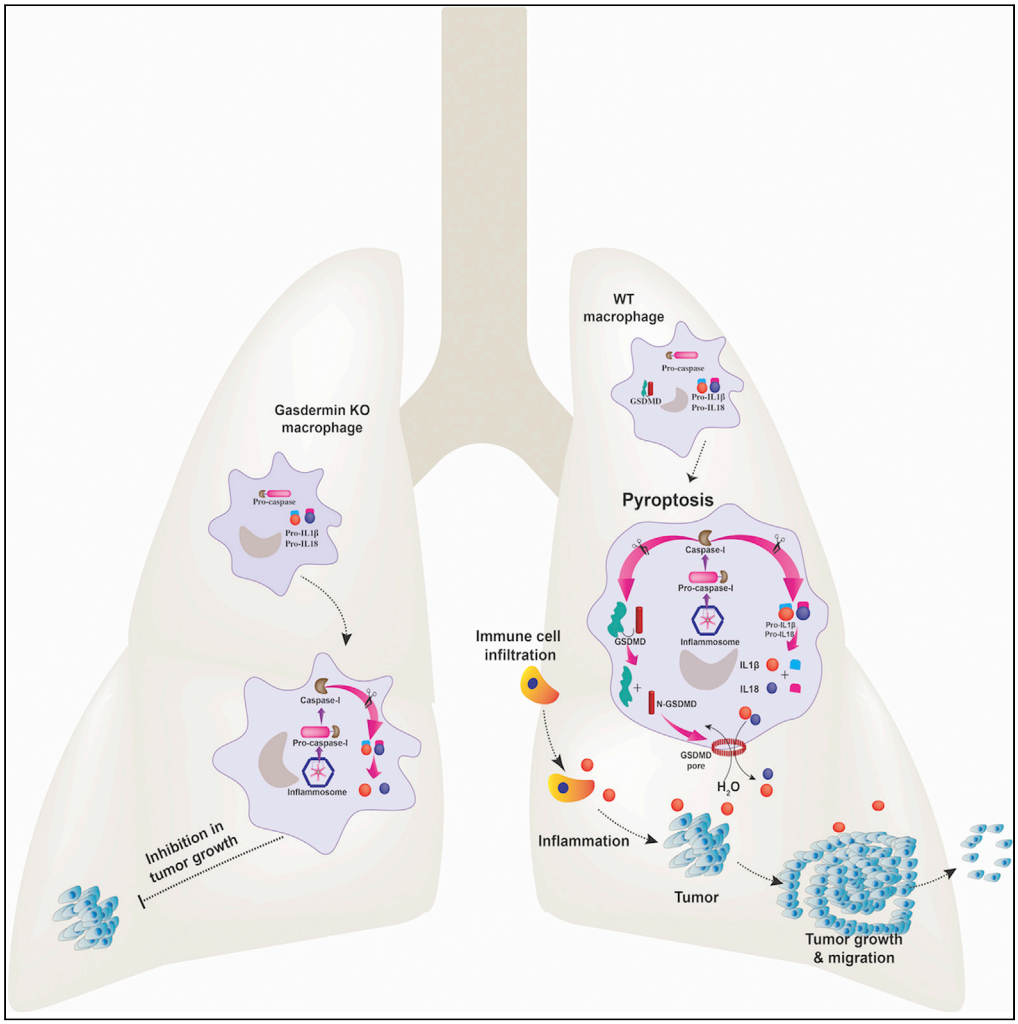

C. Alicia Traughber, Gauravi M. Deshpande, Kalash Neupane, ..., Jonathan D. Smith, Laura E. Nagy, Kailash Gulshan

k.gulshan@csuohio.edu

Highlights

GsdmD promoted lung cancer in syngeneic LLC mouse model of metastatic lung cancer

GsdmD promoted macrophage infiltration and promoted cancer cell migration and growth

LLC tumor-bearing GsdmD KO mice showed an increased median survival

GsdmD promoted lung cancer in a myeloid cell-specific manner

Traughber et al., iScience *26*, 106076
February 17, 2023
https://doi.org/10.1016/j.isci.2023.106076

iScience

CellPress
OPEN ACCESS

Article

Myeloid-cell-specific role of Gasdermin D in promoting lung cancer progression in mice

C. Alicia Traughber,[1,2,3] Gauravi M. Deshpande,[4,7] Kalash Neupane,[1,2,7] Nilam Bhandari,[1,2,7] Mariam R. Khan,[1,2] Megan R. McMullen,[5,6] Shadi Swaidani,[3] Emmanuel Opoku,[3] Santoshi Muppala,[3] Jonathan D. Smith,[3] Laura E. Nagy,[5,6] and Kailash Gulshan[1,2,3,8,*]

SUMMARY

The activities of the NLRP3 and AIM2 inflammasomes and Gasdermin D (GsdmD) are implicated in lung cancer pathophysiology but it's not clear if their contributions promote or retard lung cancer progression. Using a metastatic Lewis lung carcinoma (LLC) cell model, we show that GsdmD knockout (GsdmD$^{-/-}$) mice form significantly fewer cancer foci in lungs, exhibit markedly decreased lung cancer metastasis, and show a significant ~50% increase in median survival rate. The cleaved forms of GsdmD and IL-1β were detected in lung tumor tissue, indicating inflammasome activity in lung tumor microenvironment (TME). Increased migration and growth of LLC cells was observed upon exposure to the conditioned media derived from inflammasome-induced wild type, but not the GsdmD$^{-/-}$, macrophages. Using bone marrow transplantations, we show a myeloid-specific contribution of GsdmD in lung cancer metastasis. Taken together, our data show that GsdmD plays a myeloid-specific role in lung cancer progression.

INTRODUCTION

Lung cancer accounts for only 13% of all the new cancer diagnoses but 24% of all cancer deaths, making it the leading cause of cancer deaths, with an estimated 1.8 million deaths (18%), followed by colorectal (9.4%), liver (8.3%), stomach (7.7%), and breast (6.9%) cancers.[1,2] Epidemiological studies show the role of chronic inflammation in promoting various types of cancers, including lung cancer.[3] Inflammation induced by LPS treatment promotes lung cancer growth in mice.[4] Microbiota, which serves as an endogenous source of LPS, can affect patient responses to cancer immunotherapy and commensal lung microbiota can modulate levels of Interleukin-1beta (IL-1β) in lung tumor microenvironment.[5,6] IL-1β is one of the prominent cytokines in the lung tumor microenvironment (TME), promoting tumor invasiveness and metastasis.[7–10] A retrospective study based on the CANTOS trial on human patients with CVD showed a 56% reduction in lung cancer incidence in the patients receiving anti-IL-1β antibody vs. placebo.[11–13] Activation of NLRP3 or AIM2 inflammasomes allows cleavage of pro IL-1β, followed by release of mature IL-1β in a Gasdermin D (GsdmD) dependent manner, from living as well as pyroptotic cells.[14–17] GsdmD expression was shown to be up-regulated in human non-small cell lung cancer (NSCLC) tissue, while the depletion of AIM2 or NLRP3 in lung cancer cells led to reduced growth of cells.[18–22] GsdmD belongs to the family of Gasdermin proteins containing a cytotoxic N-terminal domain and a C-terminal repressor domain shielding the N-terminal domain. After cleavage of GsdmD, the N-terminal fragment gets inserted into the plasma membrane, forming large oligomeric pores, and disrupting membrane integrity.[14,15,23,24] The cleaved N-terminal fragment of GsdmD binds to phosphatidylinositol 4,5-bisphosphate (PIP2) and phosphatidylserine (PS) on the plasma membrane, leading to pore formation, IL-1β release, and pyroptotic cell death.[15–17] Though studies have implicated inflammasome components in lung cancer,[19–22] but the direct role of GsdmD in lung cancer progression in mouse models or human patients has not yet been explored. We used a syngeneic Lewis Lung Carcinoma (LLC) mouse model, which entails the injection of immunologically compatible cancer cells into fully immunocompetent mice, to determine the role of GsdmD in lung cancer progression. The LLC cell line is highly tumorigenic and is primarily used to model metastasis, being the most used and highly reproducible syngeneic model for lung cancer to date. Furthermore, the LLC model has been successfully used as a preclinical model for evaluating the efficacy of anticancer drugs.[25] Here, we tested the role of GsdmD in recipient mice that were injected with LLC on

[1]Center for Gene Regulation in Health and Disease, Cleveland State University, Cleveland, OH 44115, USA

[2]Department of Biology, Geology, and Environmental Sciences, Cleveland State University, Cleveland, OH 44115, USA

[3]Department of Cardiovascular & Metabolic Sciences, Lerner Research Institute, Cleveland Clinic, Cleveland, OH 44195, USA

[4]Digital Imaging Core, Lerner Research Institute, Cleveland Clinic, Cleveland, OH 44195, USA

[5]Departments of Inflammation and Immunity and Gastroenterology/Hepatology, Lerner Research Institute, Cleveland Clinic, Cleveland, OH 44195, USA

[6]Northern Ohio Alcohol Center, Cleveland Clinic, Cleveland, OH 44195, USA

[7]These authors contributed equally

[8]Lead contact

*Correspondence: k.gulshan@csuohio.edu

https://doi.org/10.1016/j.isci.2023.106076

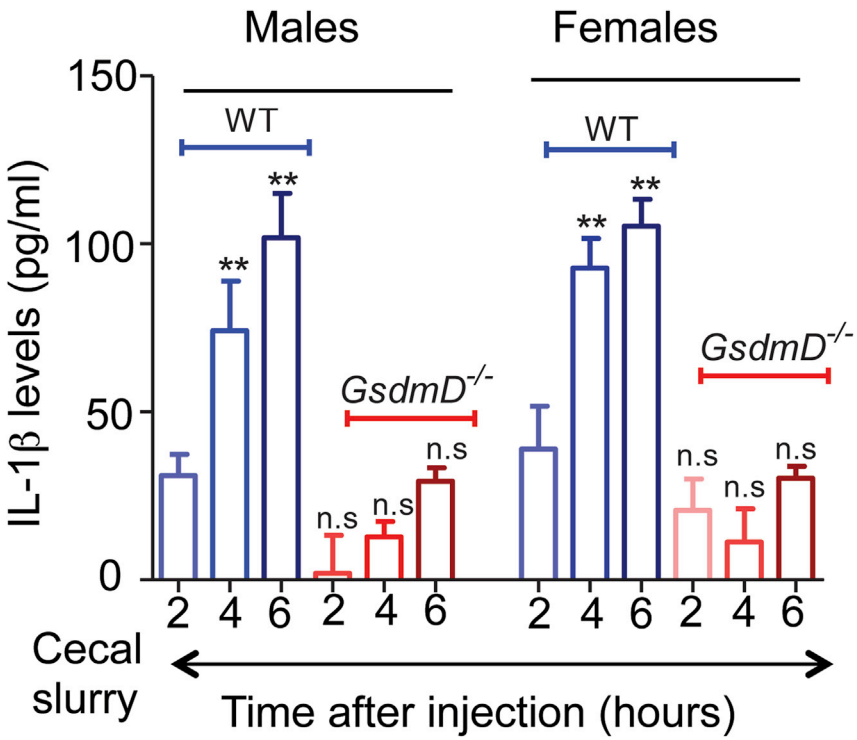

Figure 1. Defective IL-1β release in GsdmD$^{-/-}$ mice upon systemic inflammation

IL-1β ELISA showing levels of plasma IL-1β in WT and GsdmD$^{-/-}$ mice (aged 11–12 weeks, both sexes) at indicated time periods post cecal slurry injection. Data plotted as mean ± SD with N = 5 for both males and females, ** show $p < 0.01$ by ANOVA Bonferroni posttest. n.s. = non-significant.

lung cancer progression. We performed bone marrow transplantation (BMT) to determine the myeloid cell-specific contribution of GsdmD in promoting LLC tumor progression in mice.

RESULTS

Defective IL-1β release in GsdmD$^{-/-}$ mice in polymicrobial cecal slurry-induced sepsis model

Previous studies have shown that GsdmD$^{-/-}$ mice are protected against LPS-induced mortality and are defective in IL-1β release upon inflammasome activation.[14,26] To determine if GsdmD plays a role in the release of IL-1β upon microbial-induced inflammation, we used a polymicrobial cecal slurry injection mouse model.[27] Age and sex-matched C57BL6J-WT and GsdmD$^{-/-}$ mice were injected i.p. with a standardized pool of cryopreserved mouse cecal slurry (4 μL/g body weight). This dose of cecal slurry was selected based on pilot data showing that it did not induce rapid mortality, but still led to a transient decrease in body temperature to 35°C. The IL-1β in plasma at 4h and 6h post-injection increased significantly in WT mice, while the GsdmD$^{-/-}$ mice showed a minimal increase in plasma IL-1β levels (Figure 1). These data indicate that GsdmD plays a role in microbial-induced IL-1β release in the host.

GsdmD$^{-/-}$ mice show markedly reduced Lewis lung carcinoma metastasis

We tested the effect of GsdmD$^{-/-}$ on lung cancer metastasis in mice by i.v. retro-orbital (r.o) injection of LLC cells (2.5×10^5 cells per mouse). The heart and lungs were perfused and the visible tumor foci on the lungs were counted. The GsdmD$^{-/-}$ mice showed significantly fewer lung tumor metastatic foci vs. WT mice, with similar effects in both males and females (Figures 2A, S1A, S1B). The H & E staining of lung sections from WT mice showed robust cancer growth, while GsdmD$^{-/-}$ mice showed significantly reduced cancer growth (Figures 2B, S2A, and S2B). The Masson trichrome staining of WT lung sections showed robust collagen deposition, while GsdmD$^{-/-}$ mice showed significantly reduced collagen deposition (Figures 2C and S3). Quantification of the total tumor area and collagen deposition in lung sections showed a marked reduction in % tumor area and collagen deposition in GsdmD$^{-/-}$ mice (Figures 2D and 2E). These data indicate that GsdmD plays a role in lung cancer growth and collagen deposition in cancerous tissue.

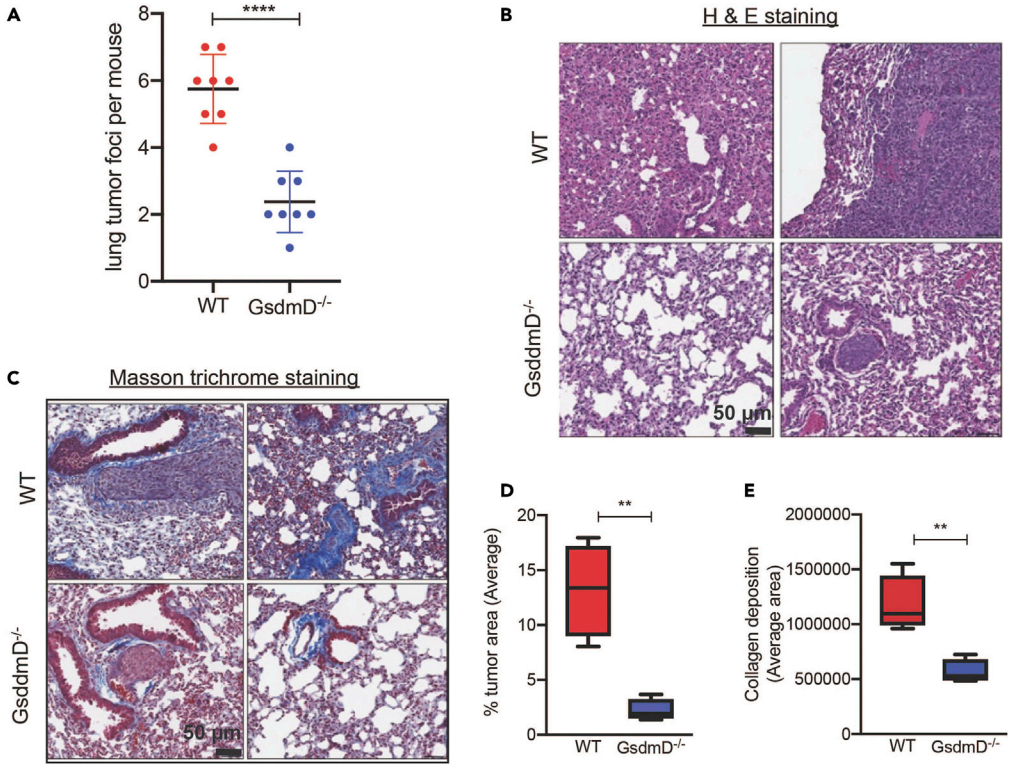

Figure 2. GsdmD$^{-/-}$ mice show reduced lung cancer metastasis

(A) Quantification of metastatic foci in lungs from WT and GsdmD$^{-/-}$ mice (aged 11–12 weeks, n = 8, 4 females, 4 males per strain), ****p=<0.0001, two-tailed t-test.

(B) Representative H&E staining of lung sections showing tumor growth in WT and GsdmD$^{-/-}$ mice.

(C) Representative Masson trichrome staining showing collagen deposition in lung sections from tumor-bearing WT and GsdmD$^{-/-}$ mice.

(D) Quantification of % tumor area with bar showing the average of 4 different sections from WT and GsdmD$^{-/-}$ mice. **p = 0.0024, two-tailed t-test.

(E) Quantification of collagen deposition with bar showing the average of different 4 sections WT and GsdmD$^{-/-}$ mice. **p = 0.0048, two-tailed t-test.

Lewis lung carcinoma tumor-bearing GsdmD$^{-/-}$ mice show increased survival

To determine if reduced lung cancer metastasis can lead to increased median survival, we performed a Kaplan-Meier survival curve analysis on LLC tumor-bearing WT and GsdmD$^{-/-}$ mice. The mice were injected r.o. with 2.5 × 10^5 LLC cells and were followed until moribund (a marked decrease in body weight, hypothermia, or other conditions requiring immediate euthanasia) or death. The WT mice showed a median survival of ~12 days, while the GsdmD$^{-/-}$ mice showed a significantly higher median survival of ~18 days (Figure 3). An independent experiment showed similar results with GsdmD$^{-/-}$ mice showing increased median survival rate vs. WT mice (Figure S4A). These data indicated that GsdmD promoted lung cancer mortality in mice.

Inflammasome activity in lung tumor microenvironment

Various studies have indirectly implicated inflammasomes in lung cancer pathophysiology.[20,21,28] To gather evidence for inflammasome activity, the tumor tissue protein extracts were probed with antibodies that recognize the cleaved forms of IL-1β and GsdmD, but not the full-length proteins. As a control, adjacent healthy lung tissue was used. As shown in Figures 4A and 4B, the cleaved forms of IL-1β and GsdmD were present only in the lysates prepared from tumor tissue, but not from the adjacent healthy lung tissue. The GsdmD expression in tumor tissue was also confirmed by another mouse-specific antibody against cleaved GsdmD (Figure S4B). The levels of IL-1β in tumor tissue of WT mice were also significantly higher than in adjacent healthy lung tissue (Figure S4C). These data indicate the presence of functional inflammasome activity in the lung TME.

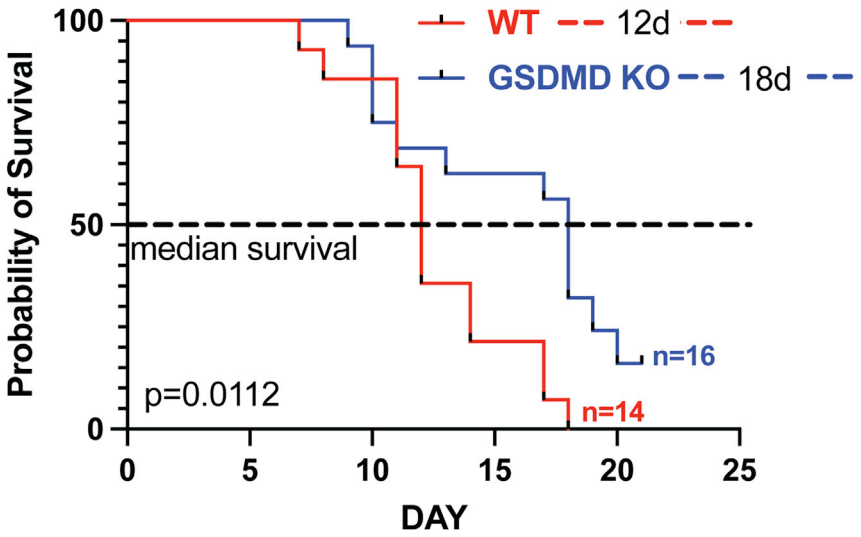

Figure 3. LLC tumor-bearing GsdmD$^{-/-}$ mice show increased survival

Male WT C57BL6J and GsdmD$^{-/-}$ mice were r.o. injected with 2.5 × 10^5 cells and the survival of mice was determined over period of 25 days. N = 14 for WT mice and N = 16 for GsdmD$^{-/-}$ mice, p = 0.0112 by Log-rank test.

To determine if injected LLC cells are contributing to inflammasome activity in lung TME, we probed LLC cell extract with antibodies against various inflammasome components. The western blot showed expression of AIM2 but there was no detectable expression of Nlrp3 (Figure 4B). Other inflammasome components such as caspase 1, IL-1β, and ASC adaptor were also not expressed in LLC cells. Murine RAW264.7 macrophages used as positive control showed basal and LPS-induced expression of all inflammasome components, including Nlrp3, caspase 1, IL-1β, and ASC. We also tested Nlrp3 expression in LLC cells by qRT-PCR and as shown in Figure 4C, LLC cells do not express detectable NLRP3 mRNA. In agreement with western blot results, qRT-PCR analysis showed expression of AIM 2 transcript (Figure 4D). Taken together, these data indicate that LLC cells do not express Nlrp3 or other inflammasome components, though a basal level of AIM2 expression is maintained. To determine if the presence of cleaved GsdmD and IL-1β is due to increased immune cell infiltration, we performed Mac3 staining to probe the levels of macrophages in TME. The LLC tumor-bearing WT mice showed a marked increase in macrophage infiltration in TME as compared to adjacent healthy tissue (Figures 4E, 4F, S4D). In contrast to WT mice, the GsdmD$^{-/-}$ mice showed a severe reduction in macrophage infiltration (Figures 4E, 4F, S4D). Thus, GsdmD may promote lung cancer growth by promoting levels of tumor-associated macrophages (TAMs).

Inflammasome-induced macrophages induced cancer cell growth

The growth of lung cancer can be modulated by a variety of factors released in TME by host immune cells as well as by cancer cells. To determine if inflammasome-induced macrophages can modulate cancer cell growth, conditioned media derived from inflammasome-induced WT or GsdmD$^{-/-}$ BMDMs was used. The assembly of NLRP3 or AIM2 inflammasome was induced by treatment with LPS + ATP or with LPS + dA:dT, as described earlier.[26,29] As shown in Figure 5A, LLC cells incubated with conditioned media from AIM2 inflammasome-induced WT BMDMs induced cell growth by ~ 30%. In contrast, the conditioned media isolated from GsdmD$^{-/-}$ BMDMs failed to show similar robust effects on cell growth. These data indicate that inflammasome assembly in macrophages in lung TME can promote cancer cell growth.

Inflammasome-induced macrophages induced cancer cell migration

To determine the mechanism by which inflammasome activation can enhance lung cancer metastasis, the effect of conditioned media derived from inflammasome-induced BMDMs was tested on trans-well migration of LLC cells. The starved LLC were treated with either conditioned media from WT BMDMs or GsdmD$^{-/-}$ BMDMs, and cells were allowed to migrate for 24h. The control cells were left untreated. As shown in Figure 5B, the conditioned media from inflammasome-induced WT macrophages increased the trans-well migration of LLC cells, while the conditioned media derived from inflammasome-induced GsdmD$^{-/-}$ macrophages failed to show similar effects. To determine if the increased migration of LLC is

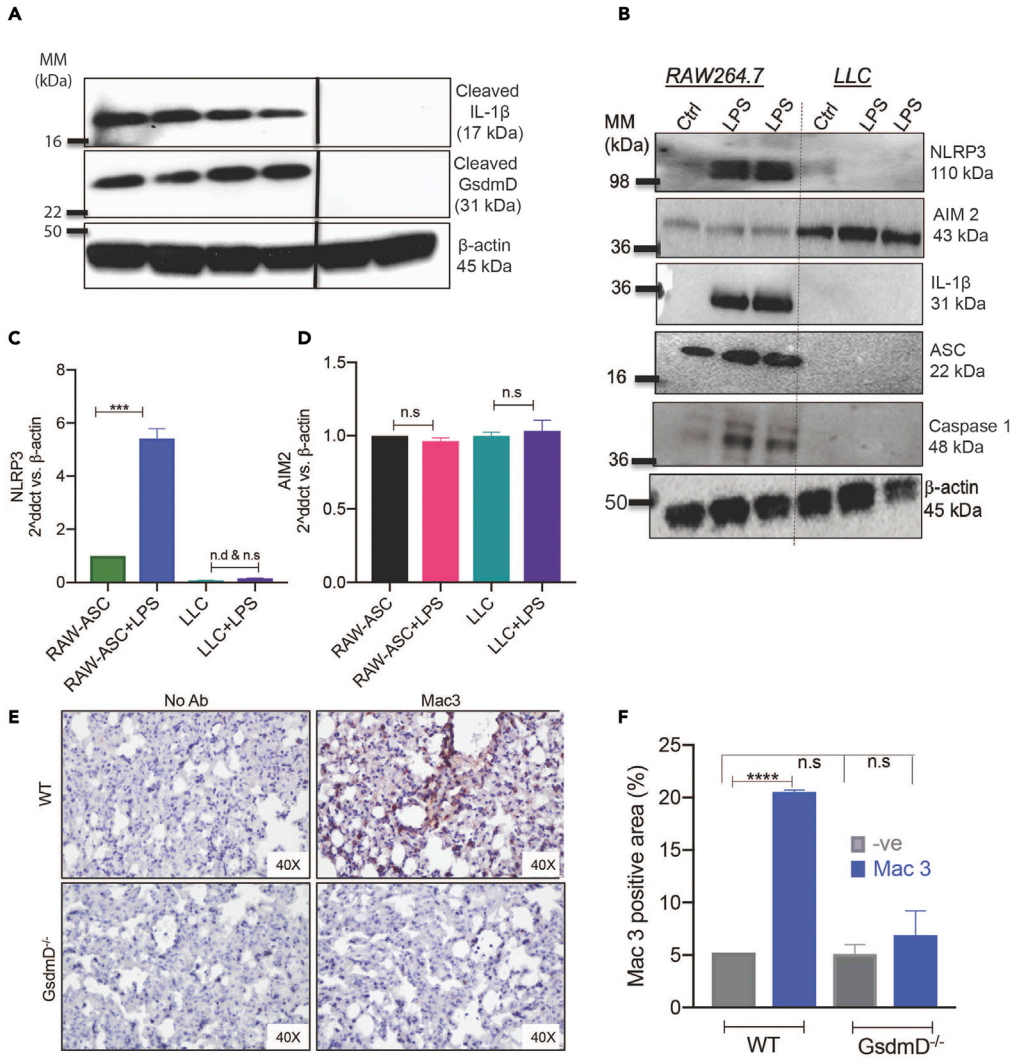

Figure 4. Expression of cleaved GsdmD in lung TME

(A) Western blot analysis of protein extracts from lung tumor tissue and adjacent healthy lung tissue, probed with mouse-specific antibodies against cleaved form of IL-1β and GsdmD. β-actin was used as a control.

(B) Western blot analysis for various inflammasome components from LLC cell extracts ± LPS treatment or from RAW-ASC cells ± LPS treatment.

(C) qRT-PCR gene expression analysis of NLRP3 and (D) AIM2 in LLC and RAW-ASC cells. N = 3, mean ± SD, ***$p < 0.001$, n.d = not defined (below detection levels), n.s = non-significant.

(E) Mac3 staining for macrophage infiltration in lung tumor sections (40X magnification) from WT and GsdmD$^{-/-}$ mice, with no antibody controls.

(F) Quantification of Mac3 staining using three independent areas, mean ± SD, ***$p < 0.001$, n.s = not significant, with ordinary one-way ANOVA posttest.

indeed due to IL-1β, the conditioned media derived from WT BMDMs was pretreated with antibodies against the cleaved form of IL-1β. As shown in Figure 5B, anti-IL-1β antibody treatment reduced LLC cell migration. These data indicate that the IL-1β released from the inflamed macrophages induced LLC cell migration. We also tested the effect of conditioned media derived from the inflammasome-activated human THP-1 cells on the migration of human A549 lung cancer cells. The cell migration was determined qualitatively as well as quantitatively via wound healing assay using live-cell video microscopy. As shown in Figures 6A and 6B, A549 cell migration in the presence of conditioned media derived from inflamed THP-1 macrophages or recombinant human IL-1β was significantly faster than control cells. Representative video microscopy movies are shown in Figures S5, S6, and S7. The cell migration effect of conditioned media from

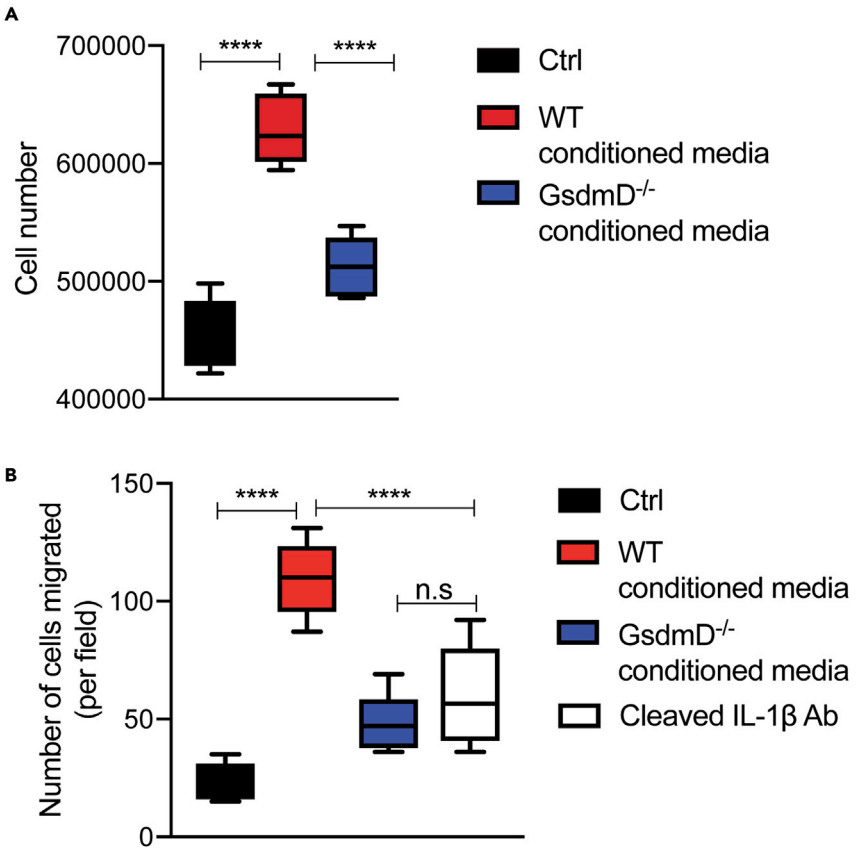

Figure 5. Inflammasome-induced macrophages promoted LLC cell growth and migration

(A) LLC cell growth assay with conditioned media from inflamed WT or GsdmD$^{-/-}$ macrophages, control cells are treated with conditioned media from non-stimulated cells (N = 5, whiskers are minimum to maximum, ****represent $p < 0.0001$ for Ctrl vs. WT conditioned media and WT conditioned media vs. GsdmD$^{-/-}$ conditioned media, while Ctrl vs. GsdmD$^{-/-}$ conditioned media showed *, $p = 0.0221$ with ANOVA using Tukey's multiple comparisons test.

(B) LLC cell trans-well assay migration with conditioned media from inflamed WT or GsdmD$^{-/-}$ macrophages or with WT conditioned media pretreated with antibody against cleaved IL-1β, control cells are treated with conditioned media from non-stimulated cells (N = 6, mean ± SD, ****represent $p < 0.0001$ for Ctrl vs. WT conditioned media, ****represent $p < 0.0001$ for WT conditioned media vs. GsdmD$^{-/-}$ conditioned media, and ****represent $p < 0.0001$ for WT conditioned media vs. cleaved IL-1β, while Ctrl vs. cleaved IL-1β showed **, $p = 0.0025$, Ctrl vs. GsdmD$^{-/-}$ conditioned media showed *, $p = 0.0408$, and GsdmD$^{-/-}$ conditioned media vs. cleaved IL-1β showed no significant difference (n.s.) with ANOVA using Tukey's multiple comparisons test.

inflamed macrophages was also confirmed in other lung cancer cell lines (Figures S8A and S8B). Matrix metalloproteinases, such as MMP9. are known to be upregulated and activated during cell migration and plays a role in tumor invasion.[30] The MMP9 expression was induced in A549 cells exposed to conditioned-media derived from inflamed macrophages vs. conditioned media from control macrophages (Figure S8C). These data indicated that cytokine release from inflammasome-induced immune cells in TME could induce lung cancer cell migrations and metastasis.

Myeloid cell-specific role of Gasdermin D in lung cancer

To determine if the role of GsdmD in promoting lung cancer is myeloid-cell specific, we performed bone marrow transplant (BMT) assays. A 100% success rate for BMT was achieved, with all the WT mice transplanted with GsdmD$^{-/-}$ bone marrow cells showing the presence of GsdmD$^{-/-}$ myeloid cells in the blood. The BMT strategy and representative successful BMTs are shown in Figures 7A and 7B. The 11–12 weeks old male WT mice, transplanted with either WT or GsdmD$^{-/-}$ bone marrow, were given r.o. injection of LLC cells as described above. Mice were followed for survival; endpoints sudden death, moribund, or respiratory distress. As shown in Figure 7C, the mice transplanted with GsdmD$^{-/-}$ BMT showed a significantly

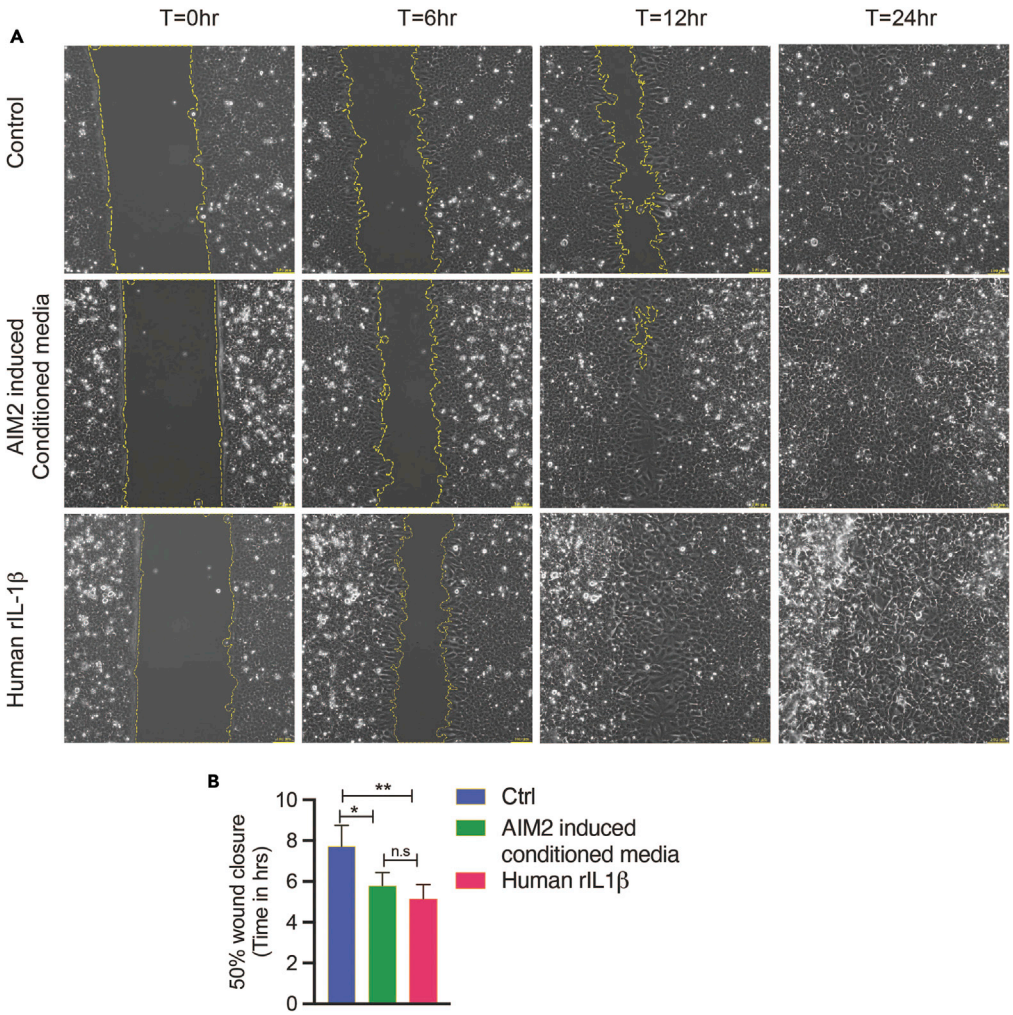

Figure 6. Inflammasome activated THP-1 macrophages promoted the migration of human lung cancer cells

(A) Representative images from human A549 cells migration in a wound healing assay with conditioned media from AIM2 inflammasome-induced human THP-1 macrophages or human recombinant IL-1β protein. Control cells are treated with conditioned media from non-stimulated cells.

(B) The $T_{1/2}$ (half-time) was calculated via live cell video microscopy and plot shows the average of each sample (n = 4, mean ± SD, **represent p = 0.0029, *represent p = 0.0163, and n.s = non-significant, with ANOVA using Tukey's multiple comparisons test.

higher survival rate vs. mice transplanted with WT BMT. These data provide the first evidence for the myeloid cell-specific role of GsdmD in promoting lung progression.

DISCUSSION

Contribution of inflammatory pyroptotic cell death in lung cancer progression and metastasis is not clear. Epidemiological studies show the role of chronic inflammation in promoting various types of cancers, including lung cancer.[3] Mature IL-1β can be generated by the activation of NLRP3 or AIM2 inflammasome. The role of inflammasome in human lung cancer was also highlighted by gene expression analysis of nonhematopoietic bone marrow niche cells from *Kras*^{G12D} mice, showing the upregulation of multiple inflammation-related genes including IL-1β and the NLPR3 inflammasome.[31]

Activation of inflammasomes allows caspase1/11-mediated cleavage of GsdmD in immune cells.[14,15] The N-terminal fragment of GsdmD is recruited to the plasma membrane, leading to pore formation, IL-1β release, and pyroptotic cell death.[15–17] Intriguingly, GsdmD is also involved in the release of mature

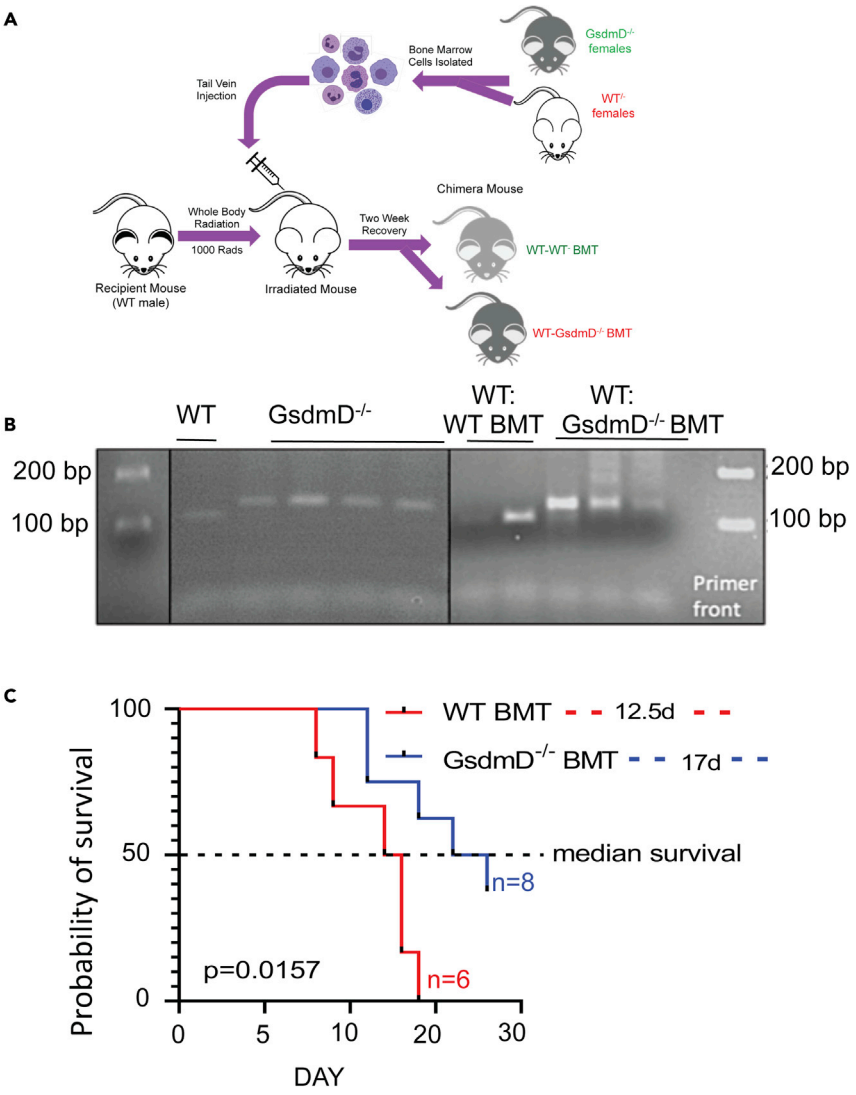

Figure 7. Myeloid-specific role of GsdmD in lung cancer

(A) Schematic diagram showing BMT strategy. Bone marrow cells were collected from WT or GsdmD$^{-/-}$ females and irradiated WT male mice were injected with bone marrow cells from either WT or GsdmD$^{-/-}$ mice by tail-vein injection.

(B) PCR confirming WT or GsdmD$^{-/-}$ BMT. GsdmD$^{-/-}$ contains 20bp (19bp + 1bp) insertion and the WT sequence "ATGTTGTCAGG" is mutated to "ATGcTTGaaggtgtgtggatgcagagTCAGG".

(C) Survival of WT-WT BMT and WT-GsdmD$^{-/-}$ BMT mice with LLC tumors. N = 6 for WT- WT-BMT n = 6, and N = 8 for WT-GsdmD$^{-/-}$-BMT, p = 0.0157, by Log-rank test.

IL-1β from living macrophages,[32] indicating role of GsdmD in inflammation is not limited to pyroptosis. Thus, the role of GsdmD from the TME in supporting lung cancer progression may be independent of pyroptosis. The Gasdermin protein family is conserved among vertebrates and is comprised of six members in humans, GsdmA, GsdmB, GsdmC, GsdmD, GsdmE, and DFNB59. Gasdermin proteins are expressed in a variety of cell types including epithelial and immune cells and their role in cancer in diverse, with some members exhibiting tumor-promoting properties, while others act to inhibit tumor growth. GsdmE was recently identified as a tumor suppressor in melanoma, breast cancer, and colorectal tumor.[33] GsdmB was shown to promote breast cancer.[34,35] while PD-L1-mediated GsdmC expression was shown to cause a switch from apoptosis to pyroptosis in cancer cells to facilitate tumor necrosis.[36] The role of GsdmD in lung cancer is not consistent across different studies. Multiple studies have shown that depleting the levels of AIM2, NLRP3, or GsdmD in lung cancer cells can inhibit cell growth,[19–22] but the direct role of GsdmD in lung cancer is not fully clear. GsdmD expression was shown to be upregulated in human non-small cell lung

cancer (NSCLC) tissue and GsdmD depletion reduced lung cancer growth.[18] In contrast, GsdmD was found to be essential for an optimal cytotoxic T-cells response to cancer cells,[37] indicating the tumor-inhibiting activity of GsdmD. Another elegant study showed the role of IL-1β in lung cancer growth independent of NLRP3 inflammasome, with no effect of GsdmD knockout on lung cancer growth in a skin-graft model.[38] We aimed to determine the *in vivo* role of GsdmD in promoting cancer cell growth in the lungs. Using the metastatic LLC cell model, we found that the knockout of GsdmD in mice markedly reduced LLC cancer progression in lungs (Figures 2, 3). Given that the injected LLC cells were not engineered, it is the host GsdmD that supports lung cancer progression. The GsdmD$^{-/-}$ mice showed significantly reduced collagen deposition in cancer tissue vs. WT mice (Figure 3). Collagen in lung TME promotes fibrosis and metastasis of cancer. GsdmD has been proposed to increase collagen production in skin fibrosis,[39] thus GsdmD$^{-/-}$ may be producing less collagen in lung TME, leading to attenuated tumor growth. The GsdmD$^{-/-}$ mice exhibited significantly increased survival upon LLC cell injection vs. WT cells, indicating that GsdmD inhibition may serve as stand-alone or adjuvant therapy to treat lung cancer.

Previous studies implicated inflammasomes in lung cancer cell growth.[18,20,21,28] We found the robust activity of inflammasome in lung cancer tissue. Interestingly, the LLC cells do not express Nlrp3 or other inflammasome components. Expression of Aim2 was detected in LLC cells but the injected cancer cells may not directly contribute to inflammasome activity in lung TME due to the lack of expression of inflammasome components. (Figure 4) The likelihood of inflammasome activity being regulated by immune cells in TME is more plausible rather than lung epithelium being the source of inflammasome activity. Though unlikely, the contribution of host lung epithelial tissue in the expression of inflammasome components in cancer tissue cannot be completely ruled out. AIM2 is a receptor that recognizes cytosolic foreign DNA via intracellular Toll-like receptors (TLRs) 7 and 9. One possibility is that DNA from dying cancer cells or DNA fragments from neutrophil extracellular traps (NETosis) are released in lung TME, which are engulfed by macrophages and dendritic cells, allowing the activation of AIM2 via TLR7/9. The AIM2 in LLC cells may also get activated by DNA from nearby damaged cells, but the consequences of this activation are most likely to be independent of inflammasome activity.

The presence of cleaved GsdmD in LLC tumor tissue (Figure 4) points toward inflammasome activity in lung TME. Though the presence of cleaved GsdmD indicates functional inflammasome, it does not provide foolproof evidence for pyroptosis induced IL-1β in tumor tissue, as living macrophages can also release mature IL-1β.[32] Furthermore, cells can release IL-1β in a GsdmD dependent as well as GsdmD independent manner.[17,40] One clear evidence for GsdmD mediated modulation of immune-cell profile in lung TME came from data showing markedly reduced levels of tumor-associated macrophages (TAMs) in GsdmD$^{-/-}$ vs. WT mice (Figure 4E). TAMs are known to play role in the angiogenesis, progression, and metastasis of lung cancer. Furthermore, TAMs confer chemotherapy resistance and immunosuppression. GsdmD-mediated pyroptotic cell death in TME can result in a sharp increase of pro-inflammatory cytokine and other danger signals. These signals can result in a continuous influx of immune cells, such as tumor-associated macrophages (TAMs), resulting in suppression of host anti-tumor responses. The high density of TAMs in lung cancer correlates with reduced overall patient survival and depletion of TAMs slows lung tumor growth in mice.[41,42] The immunosuppressive role of myeloid-derived suppressor cells (MDSCs) is getting increasingly recognized in lung cancer,[43] and the tumor-derived IL-1β has been shown to induce the accumulation of MDSCs with enhanced capacity to suppress T cells and Natural killer (NK) cells.[44] GsdmD is expressed in almost all human organs and tissues including various subsets of leukocytes, while in mice GsdmD is expressed in the gut, colon, urinary tract heart, liver, and lungs. It's not clear if GsdmD plays a tissue-specific role in promoting lung cancer growth, or which organs are directly involved in GsdmD-mediated promotion of lung cancer growth. The function of GsdmD in immune cells is widely studied in the context of bacterial infection but the immune cell-specific role of GsdmD in promoting cancer is not known. We found that GsdmD promotes cancer growth in myeloid cell-specific manner (Figure 7). GsdmD activation in lung TME can result in an acute rise in IL-1β and other danger signals. High levels of IL-1β in the lung TME can enhance the recruitment of tumor-infiltrating macrophages (TAMs), which are known to promote lung cancer progression and suppress host anti-tumor responses.[45] High density of TAMs in lung cancer correlates with reduced overall patient survival and depletion of TAMs slows lung tumor growth in mice.[41,42] We showed the myeloid cell-specific role of GsdmD in lung cancer progression, but we cannot entirely rule out the possibility of indirect effects of myeloid GsdmD via the modulation of gut or lung microbiota. An elegant study showed that commensal bacteria stimulated MyD88-dependent IL-1β and IL-23 production from myeloid cells.[6] There is a possibility of lung microbiota being affected

in WT mice with GsdmD$^{-/-}$ BMT vs. WT mice with WT BMT. GsdmD, due to its bactericidal activity, may tilt the lung microbiota population toward a cancer-promoting rather than healthy microbiota profile.

Targeting GsdmD along with IL-1β may serve as a better adjuvant therapy than targeting IL-1β alone, as GsdmD blockage can prevent not only the IL-1β release, but can also prevent highly inflammatory pyroptotic cell death, formation of neutrophils extracellular traps, and leakage of other pro-inflammatory cytokines and cellular material in the lung TME. GsdmD inhibition may also reduce lung cancer by inducing apoptosis in inflamed TAMs. Recent studies from our group and others have shown that GsdmD$^{-/-}$ macrophages are more susceptible to apoptosis under inflammatory conditions, such as overload of cholesterol.[26,46] Thus, the inflammatory environment of lung TME may promote apoptosis in GsdmD$^{-/-}$-TAMs vs. highly inflammatory pyroptotic cell death in WT-TAMs.

The mechanistic details of inflammasome-GsdmD-IL-1β nexus in promoting lung cancer are still not fully clear. The cross-talk between GsdmD activity in macrophages, neutrophils, and other immune cells such as Tregs can modulate the host response to cancerous growth in lungs, but delineating the intricate details of the regulatory network involved in this process requires further studies.

Limitations of the study

Though our study showed the role of GsdmD in lung cancer, it did not provide evidence that reduced inflammation is the mechanism by which GsdmD knockout reduces lung cancer growth in mice. The study did not provide evidence for any specific cell type in mediating GsdmD effects on lung cancer growth. The study did not show if plasma or TME levels of IL-1β are responsible for tumor growth. We did not provide direct evidence for pyroptotic cell death in lung TME. We believe that the mechanism of GsdmD anti-lung cancer activity involves multiple cell types (such as macrophages, T cells, and others) and mechanisms (such as inflammasome activity, lung microbiota, and pyroptosis). Further studies are needed, especially with GsdmD-IL-1β double KO mouse model.

STAR★METHODS

Detailed methods are provided in the online version of this paper and include the following:

- KEY RESOURCES TABLE
- RESOURCE AVAILABILITY
  - Lead contact
  - Materials availability
  - Data and code availability
- METHOD DETAILS
  - Cell lines and BMDMs
  - Mice maintenance/diet
  - LLC metastasis R.O injection model
  - Cell migration assay
  - Wound healing assay
  - Trichrome/H&E staining and quantification
  - Mac-3 staining for macrophage infiltration
  - Western blotting
  - qRT-PCR assays
  - Generation of myeloid-specific KO of GsdmD in mice
  - Quantification and statistical analysis

SUPPLEMENTAL INFORMATION

Supplemental information can be found online at https://doi.org/10.1016/j.isci.2023.106076.

ACKNOWLEDGMENTS

This research was supported by Case Comprehensive Cancer Center (NCI comprehensive center) pilot grant and Cleveland State University startup funds to K.G. K.G is supported NIH-NHLBI grant R01-158148.

AUTHOR CONTRIBUTIONS

KG conceptualized the work and designed the study. KG and CAT designed and conducted the majority of experiments. GMP and SM assisted with microscopy, live cell video microscopy, and analysis of the images. KN, NB, MRK, and EO conducted mice and cell-based experiments. MRM and SS assisted in bone marrow transplants and survival studies. LE and JDS provided material support. KG drafted the article and all authors contributed to writing the article.

DECLARATION OF INTERESTS

The authors declare no competing interests.

INCLUSION AND DIVERSITY

One or more of the authors of this paper self-identifies as an underrepresented ethnic minority in their field of research or within their geographical location. One or more of the authors of this paper self-identifies as a gender minority in their field of research.

Received: September 15, 2022
Revised: November 29, 2022
Accepted: January 24, 2023
Published: January 31, 2023

REFERENCES

1. Bray, F., Ferlay, J., Soerjomataram, I., Siegel, R.L., Torre, L.A., and Jemal, A. (2018). Global cancer statistics 2018: GLOBOCAN estimates of incidence and mortality worldwide for 36 cancers in 185 countries. CA. Cancer J. Clin. *68*, 394–424.

2. Sung, H., Ferlay, J., Siegel, R.L., Laversanne, M., Soerjomataram, I., Jemal, A., and Bray, F. (2021). Global cancer statistics 2020: GLOBOCAN estimates of incidence and mortality worldwide for 36 cancers in 185 countries. CA. Cancer J. Clin. *71*, 209–249.

3. Mantovani, A., Allavena, P., Sica, A., and Balkwill, F. (2008). Cancer-related inflammation. Nature *454*, 436–444.

4. Melkamu, T., Qian, X., Upadhyaya, P., O'Sullivan, M.G., and Kassie, F. (2013). Lipopolysaccharide enhances mouse lung tumorigenesis: a model for inflammation-driven lung cancer. Vet. Pathol. *50*, 895–902.

5. Routy, B., Le Chatelier, E., Derosa, L., Duong, C.P.M., Alou, M.T., Daillère, R., Fluckiger, A., Messaoudene, M., Rauber, C., Roberti, M.P., et al. (2018). Gut microbiome influences efficacy of PD-1-based immunotherapy against epithelial tumors. Science *359*, 91–97.

6. Jin, C., Lagoudas, G.K., Zhao, C., Bullman, S., Bhutkar, A., Hu, B., Ameh, S., Sandel, D., Liang, X.S., Mazzilli, S., et al. (2019). Commensal microbiota promote lung cancer development via gammadelta T cells. Cell *176*, 998–1013.e16.

7. Voronov, E., Shouval, D.S., Krelin, Y., Cagnano, E., Benharroch, D., Iwakura, Y., Dinarello, C.A., and Apte, R.N. (2003). IL-1 is required for tumor invasiveness and angiogenesis. Proc. Natl. Acad. Sci. USA *100*, 2645–2650.

8. Tu, S., Bhagat, G., Cui, G., Takaishi, S., Kurt-Jones, E.A., Rickman, B., Betz, K.S., Penz-Oesterreicher, M., Bjorkdahl, O., Fox, J.G., and Wang, T.C. (2008). Overexpression of interleukin-1beta induces gastric inflammation and cancer and mobilizes myeloid-derived suppressor cells in mice. Cancer Cell *14*, 408–419.

9. Song, X., Krelin, Y., Dvorkin, T., Bjorkdahl, O., Segal, S., Dinarello, C.A., Voronov, E., and Apte, R.N. (2005). CD11b+/Gr-1+ immature myeloid cells mediate suppression of T cells in mice bearing tumors of IL-1beta-secreting cells. J. Immunol. *175*, 8200–8208.

10. Saijo, Y., Tanaka, M., Miki, M., Usui, K., Suzuki, T., Maemondo, M., Hong, X., Tazawa, R., Kikuchi, T., Matsushima, K., and Nukiwa, T. (2002). Proinflammatory cytokine IL-1 beta promotes tumor growth of Lewis lung carcinoma by induction of angiogenic factors: in vivo analysis of tumor-stromal interaction. J. Immunol. *169*, 469–475.

11. Ridker, P.M., MacFadyen, J.G., Thuren, T., Everett, B.M., Libby, P., and Glynn, R.J.; CANTOS Trial Group (2017). Effect of interleukin-1beta inhibition with canakinumab on incident lung cancer in patients with atherosclerosis: exploratory results from a randomised, double-blind, placebo-controlled trial. Lancet *390*, 1833–1842.

12. Ridker, P.M. (2021). Inhibiting interleukin-6 to reduce cardiovascular event rates: a next step for atherothrombosis treatment and prevention. J. Am. Coll. Cardiol. *77*, 1856–1858.

13. Ridker, P.M., Libby, P., MacFadyen, J.G., Thuren, T., Ballantyne, C., Fonseca, F., Koenig, W., Shimokawa, H., Everett, B.M., and Glynn, R.J. (2018). Modulation of the interleukin-6 signalling pathway and incidence rates of atherosclerotic events and all-cause mortality: analyses from the Canakinumab Anti-Inflammatory Thrombosis Outcomes Study (CANTOS). Eur. Heart J. *39*, 3499–3507.

14. Kayagaki, N., Stowe, I.B., Lee, B.L., O'Rourke, K., Anderson, K., Warming, S., Cuellar, T., Haley, B., Roose-Girma, M., Phung, Q.T., et al. (2015). Caspase-11 cleaves gasdermin D for non-canonical inflammasome signalling. Nature *526*, 666–671.

15. Ding, J., Wang, K., Liu, W., She, Y., Sun, Q., Shi, J., Sun, H., Wang, D.C., and Shao, F. (2016). Pore-forming activity and structural autoinhibition of the gasdermin family. Nature *535*, 111–116.

16. Liu, X., Zhang, Z., Ruan, J., Pan, Y., Magupalli, V.G., Wu, H., and Lieberman, J. (2016). Inflammasome-activated gasdermin D causes pyroptosis by forming membrane pores. Nature *535*, 153–158.

17. Monteleone, M., Stanley, A.C., Chen, K.W., Brown, D.L., Bezbradica, J.S., von Pein, J.B., Holley, C.L., Boucher, D., Shakespear, M.R., Kapetanovic, R., et al. (2018). Interleukin-1beta maturation triggers its relocation to the plasma membrane for gasdermin-D-dependent and -independent secretion. Cell Rep. *24*, 1425–1433.

18. Gao, J., Qiu, X., Xi, G., Liu, H., Zhang, F., Lv, T., and Song, Y. (2018). Downregulation of GSDMD attenuates tumor proliferation via the intrinsic mitochondrial apoptotic pathway and inhibition of EGFR/Akt signaling and predicts a good prognosis in nonsmall cell lung cancer. Oncol. Rep. *40*, 1971–1984.

19. Zhang, M., Jin, C., Yang, Y., Wang, K., Zhou, Y., Zhou, Y., Wang, R., Li, T., and Hu, R. (2019). AIM2 promotes non-small-cell lung cancer cell growth through inflammasome-dependent pathway. J. Cell. Physiol. *234*, 20161–20173.

20. Qi, M., Dai, D., Liu, J., Li, Z., Liang, P., Wang, Y., Cheng, L., Zhan, Y., An, Z., Song, Y., et al. (2020). AIM2 promotes the development of non-small cell lung cancer by modulating mitochondrial dynamics. Oncogene *39*, 2707–2723.

21. Wang, Y., Kong, H., Zeng, X., Liu, W., Wang, Z., Yan, X., Wang, H., and Xie, W. (2016). Activation of NLRP3 inflammasome enhances the proliferation and migration of A549 lung cancer cells. Oncol. Rep. *35*, 2053–2064.

22. Huang, L., Duan, S., Shao, H., Zhang, A., Chen, S., Zhang, P., Wang, N., Wang, W., Wu, Y., Wang, J., et al. (2019). NLRP3 deletion inhibits inflammation-driven mouse lung tumorigenesis induced by benzo(a)pyrene and lipopolysaccharide. Respir. Res. *20*, 20.

23. Kuriakose, T., and Kanneganti, T.D. (2018). Gasdermin D flashes an exit signal for IL-1. Immunity *48*, 1–3.

24. Man, S.M., Kanneganti, T.D., and Gasdermin, D. (2015). The long-awaited executioner of pyroptosis. Cell Res. *25*, 1183–1184.

25. Papageorgiou, A., Stravoravdi, P., Sahpazidou, D., Natsis, K., Chrysogelou, E., and Toliou, T. (2000). Effect of navelbine on inhibition of tumor growth, cellular differentiation and estrogen receptor status on Lewis lung carcinoma. Chemotherapy *46*, 188–194.

26. Opoku, E., Traughber, C.A., Zhang, D., Iacano, A.J., Khan, M., Han, J., Smith, J.D., and Gulshan, K. (2021). Gasdermin D mediates inflammation-induced defects in reverse cholesterol transport and promotes atherosclerosis. Front. Cell Dev. Biol. *9*, 715211.

27. Starr, M.E., Steele, A.M., Saito, M., Hacker, B.J., Evers, B.M., and Saito, H. (2014). A new cecal slurry preparation protocol with improved long-term reproducibility for animal models of sepsis. PLoS One *9*, e115705.

28. Sharma, B.R., and Kanneganti, T.D. (2021). NLRP3 inflammasome in cancer and metabolic diseases. Nat. Immunol. *22*, 550–559.

29. Iacano, A.J., Lewis, H., Hazen, J.E., Andro, H., Smith, J.D., and Gulshan, K. (2019). Miltefosine increases macrophage cholesterol release and inhibits NLRP3-inflammasome assembly and IL-1beta release. Sci. Rep. *9*, 11128.

30. Kessenbrock, K., Plaks, V., and Werb, Z. (2010). Matrix metalloproteinases: regulators of the tumor microenvironment. Cell *141*, 52–67.

31. Osswald, L., Hamarsheh, S., Uhl, F.M., Andrieux, G., Klein, C., Dierks, C., Duquesne, S., Braun, L.M., Schmitt-Graeff, A., Duyster, J., et al. (2021). Oncogenic Kras(G12D) activation in the nonhematopoietic bone marrow microenvironment causes myelodysplastic syndrome in mice. Mol. Cancer Res. *19*, 1596–1608.

32. Evavold, C.L., Ruan, J., Tan, Y., Xia, S., Wu, H., and Kagan, J.C. (2018). The pore-forming protein gasdermin D regulates interleukin-1 secretion from living macrophages. Immunity *48*, 35–44.e6.

33. Zhang, Z., Zhang, Y., Xia, S., Kong, Q., Li, S., Liu, X., Junqueira, C., Meza-Sosa, K.F., Mok, T.M.Y., Ansara, J., et al. (2020). Gasdermin E suppresses tumour growth by activating anti-tumour immunity. Nature *579*, 415–420.

34. Hergueta-Redondo, M., Sarrió, D., Molina-Crespo, Á., Megias, D., Mota, A., Rojo-Sebastian, A., García-Sanz, P., Morales, S., Abril, S., Cano, A., et al. (2014). Gasdermin-B promotes invasion and metastasis in breast cancer cells. PLoS One *9*, e90099.

35. Hergueta-Redondo, M., Sarrio, D., Molina-Crespo, Á., Vicario, R., Bernadó-Morales, C., Martínez, L., Rojo-Sebastián, A., Serra-Musach, J., Mota, A., Martínez-Ramírez, Á., et al. (2016). Gasdermin B expression predicts poor clinical outcome in HER2-positive breast cancer. Oncotarget *7*, 56295–56308.

36. Hou, J., Zhao, R., Xia, W., Chang, C.W., You, Y., Hsu, J.M., Nie, L., Chen, Y., Wang, Y.C., Liu, C., et al. (2020). PD-L1-mediated gasdermin C expression switches apoptosis to pyroptosis in cancer cells and facilitates tumour necrosis. Nat. Cell Biol. *22*, 1264–1275.

37. Xi, G., Gao, J., Wan, B., Zhan, P., Xu, W., Lv, T., and Song, Y. (2019). GSDMD is required for effector CD8(+) T cell responses to lung cancer cells. Int. Immunopharmacol. *74*, 105713.

38. Kiss, M., Vande Walle, L., Saavedra, P.H.V., Lebegge, E., Van Damme, H., Murgaski, A., Qian, J., Ehling, M., Pretto, S., Bolli, E., et al. (2021). IL1beta promotes immune suppression in the tumor microenvironment independent of the inflammasome and gasdermin D. Cancer Immunol. Res. *9*, 309–323.

39. Yang, H., Shi, Y., Liu, H., Lin, F., Qiu, B., Feng, Q., Wang, Y., and Yang, B. (2022). Pyroptosis executor gasdermin D plays a key role in scleroderma and bleomycin-induced skin fibrosis. Cell Death Discov. *8*, 183.

40. Saeki, A., Tsuchiya, K., Suda, T., Into, T., Hasebe, A., Suzuki, T., and Shibata, K.I. (2020). Gasdermin D-independent release of interleukin-1beta by living macrophages in response to mycoplasmal lipoproteins and lipopeptides. Immunology *161*, 114–122.

41. Rakaee, M., Busund, L.T.R., Jamaly, S., Paulsen, E.E., Richardsen, E., Andersen, S., Al-Saad, S., Bremnes, R.M., Donnem, T., and Kilvaer, T.K. (2019). Prognostic value of macrophage phenotypes in resectable non-small cell lung cancer assessed by multiplex immunohistochemistry. Neoplasia *21*, 282–293.

42. Fritz, J.M., Tennis, M.A., Orlicky, D.J., Lin, H., Ju, C., Redente, E.F., Choo, K.S., Staab, T.A., Bouchard, R.J., Merrick, D.T., et al. (2014). Depletion of tumor-associated macrophages slows the growth of chemically induced mouse lung adenocarcinomas. Front. Immunol. *5*, 587.

43. Yang, Z., Guo, J., Weng, L., Tang, W., Jin, S., and Ma, W. (2020). Myeloid-derived suppressor cells-new and exciting players in lung cancer. J. Hematol. Oncol. *13*, 10.

44. Elkabets, M., Ribeiro, V.S.G., Dinarello, C.A., Ostrand-Rosenberg, S., Di Santo, J.P., Apte, R.N., and Vosshenrich, C.A.J. (2010). IL-1beta regulates a novel myeloid-derived suppressor cell subset that impairs NK cell development and function. Eur. J. Immunol. *40*, 3347–3357.

45. Fritz, J.M., Tennis, M.A., Orlicky, D.J., Yin, H., Ju, C., Redente, E.F., Choo, K.S., Staab, T.A., Bouchard, R.J., Merrick, D.T., et al. (2015). Corrigendum: depletion of tumor-associated macrophages slows the growth of chemically induced mouse lung adenocarcinomas. Front. Immunol. *6*, 88.

46. Puylaert, P., Van Praet, M., Vaes, F., Neutel, C.H.G., Roth, L., Guns, P.J., De Meyer, G.R.Y., and Martinet, W. (2022). Gasdermin D deficiency limits the transition of atherosclerotic plaques to an inflammatory phenotype in ApoE knock-out mice. Biomedicines *10*, 1171.

47. Gonçalves, A.V., Margolis, S.R., Quirino, G.F.S., Mascarenhas, D.P.A., Rauch, I., Nichols, R.D., Ansaldo, E., Fontana, M.F., Vance, R.E., and Zamboni, D.S. (2019). Gasdermin-D and Caspase-7 are the key Caspase-1/8 substrates downstream of the NAIP5/NLRC4 inflammasome required for restriction of Legionella pneumophila. PLoS Pathog. *15*, e1007886.

STAR★METHODS

KEY RESOURCES TABLE

REAGENT or RESOURCE	SOURCE	IDENTIFIER
Chemicals, Peptides, and Recombinant Proteins		
RPMI-1640	Millipore Sigma	R0883
DMEM	Millipore Sigma	D0822
FBS	Gibco	10082147
2-Mercaptoethanol	Millipore Sigma	M6250
12-myrisate 13 acetate	Sigma Aldrich	P8139
Penicillin streptomycin	Cell services	721
Antigen Unmasking solution	Vector Lab	H-3301
Ethanol	Fisher Scientific	BP28184
Bovine serum albumin	Sigma Aldrich	A9647-100G
Hematoxylin and Eosin	Vector Lab	H-3401
Bloxall	Vector lab	SP-6000
Xyelene	Fisher Scientific	EW-88043-30
Diluent	Vector lab	SP-5035
Tween 20	Sigma Aldrich	P7949
EDTA free Protease Cocktail inhibitor	Thermo scientific	87785
Novex 4–20% Tris Glycine Gels	Invitrogen	XP04200BOX
LPS	Sigma Aldrich	L2880
TPER	Thermo scientific	78510
Pierce BCA	Thermo fisher	23225
Adenosine Triphosphate	Sigma Aldrich	A2383
Cell Lines		
THP-1	ATCC	TIB-202
LLC	ATCC	CRL-1642
A549	ATCC	CRM-CCL-185
RAW-ASC	Invivogen	raw-asc
Antibodies		
CD107b/Mac3	BD biosciences	550292
Cleaved Il-1beta	Cell signaling technology	63124
Cleaved Gasdermin D	Cell signaling technology	50928
Beta Actin	Cell signaling technology	8457
ASC	Cell signaling technology	67824
MMP 9	Sigma Aldrich	SCP0191
AIM2	Cell signaling technology	63660
Capsase-1	Thermo Fisher	MA5-32909
Horseradish peroxidase-Conjugated goat anti rabbit secondary	Bio Rad	1662408EDU
Critical Commercial Assays		
RNeasy Mini kit	Qiagen Inc Valencia, CA	74106
iScript cDNA kit	Bio Rad	1708891
VECTASTAIN Elite ABC-HRP kit	Vector lab	PK6104

(*Continued on next page*)

Continued

REAGENT or RESOURCE	SOURCE	IDENTIFIER
Vector NovaRed kit	Vector Lab	SK-4800
Mouse IL beta ELISA Kit	R and D systems	MLB00C
Oligonucleotides		
AIM2	Thermo Fisher	Mm01295719
NLRP3	Thermo Fisher	Mm0084094
Beta-Actin	Thermo Fisher	Mm02619580
Software and Algorithms		
Image Pro Plus	Media Cybernetics, Inc, Rockville, Maryland USA	https://www.mediacy.com/imagepro
GraphPad Prism	GraphPad	https://www.graphpad.com/
Other		
Inverted microscope	Leica Microsystems, GmbH,Wetzlar, Germany	Leica DMI6000
Hamamatsu Orca Flash4 camera	Hamamatsu Photonics, Shizuoka,Japan	Leica DMI6000
iBright^{TM} CL750 imaging system	Life Technology	A44116
QuantStudio^{TM} 3 Real -Time PCR systems	Applied Biosystem	A28137

RESOURCE AVAILABILITY

Lead contact

Information regarding this work and requests for resources and reagents should be directed to and will be fulfilled by the lead contact, Dr. Kailash Gulshan (k.gulshan@csuohio.edu).

Materials availability

This study did not generate unique reagents.

Data and code availability

This paper does not report original code.

METHOD DETAILS

Cell lines and BMDMs

THP-1 cells were cultured in RPMI medium supplemented with 10% FBS, penicillin–streptomycin antibiotics, and 0.05 mM 2- mercaptoethanol. THP-1 cells were differentiated into macrophages using 100 ng/mL phorbol 12-myristate 13-acetate (Sigma P8139) for 3 days. Bone marrow-derived macrophages (BMDMs) were generated from bone marrow cells of mice. WT or GsdmD$^{-/-}$ mice were euthanized by CO_2 inhalation and femoral bones were removed. The marrow was flushed out of the bones into a 50 mL sterile tube using a 10 mL syringe with a 26-gauge needle filled with sterile DMEM. Cells were centrifuged for 5 min at 1,800 rpm at 4°C, followed by two washes with sterile PBS. The bone marrow cells were suspended in sterile-filtered BMDM growth media (DMEM with 7.6% fetal bovine serum, 15% L-cell conditioned media, and 0.76% penicillin/streptomycin mixture) and plated in culture dishes and incubated at 37°C for 14 days. Cell media was replaced every 2–3 days for 2 weeks. The cells were routinely visualized under microscope for proliferation and differentiation into confluent BMDMs.

Mice maintenance/diet

All animal experiments were pre-approved by the Cleveland Clinic IACUC and the Cleveland State University IACUC. WT C57BL6J were purchased from The Jackson Laboratory and C57BL6J-GsdmD$^{-/-}$ mice were described before.[26,47] Mice were maintained in a temperature-controlled facility with a 12-h light/dark cycle with free access to food and water. The standard chow diet (SD, 20% kcal protein, 70% kcal carbohydrate and 10% kcal fat, Harlan Teklad) was used for regular maintenance and breeding.

LLC metastasis R.O injection model

LLC cells were cultured in regular growth media and 2.5 × 10^5 cells were injected into each mice. Male WT or GsdmD$^{-/-}$ mice (10–11 weeks of age) were put under isoflurane anesthesia and given i.v. injection into the retroorbital plexus in a volume of 0.25 mL. For injections, the skin above the eye was drawn back to protrude the eye slightly and 28-gauge needle (not to exceed ½″ to avoid trauma) was inserted at an angle of ~45°, through the inferior fornix conjunctiva membrane. The needle was gently removed to prevent injury to the eye. Eyelid was closed and mild pressure was applied to the injection site with a gauze sponge.

Cell migration assay

LLC cells were treated with conditioned media from inflammasome-induced macrophages as indicated and 5 × 10^4 cells per well were seeded in top chambers of the trans-well chamber (8 μM pore, 24-well plate, Millipore-Sigma) in FBS-free media with membrane inserts. The lower compartment contained DMEM supplemented with 10% FBS as attractant. The cells were incubated at 37°C for 24h. The cells on the lower side of the insert membrane were fixed with 5% glutaraldehyde for 10 min, followed by staining with 1% crystal violet in 2% ethanol for 30 min. The inserts were washed extensively with PBS to remove excess dye. The cells in the upper compartment of the insert were gently removed by gently wiping with a cotton swab. The insert was completely dried and the number of cells on the lower side of the filter were counted under a microscope.

Wound healing assay

Human A549 lung cancer cells were cultured and treated with vehicle, conditioned media from inflammasome-induced macrophages, or human recombinant IL-1β (rIL-1β) as indicated. Images were acquired at 10X/0.40NA, every 15 min for 24 h using a Leica DMI6000 inverted microscope (Leica Microsystems, GmbH, Wetzlar, Germany) equipped with a Hamamatsu Orca Flash4 camera (Hamamatsu Photonics, Shizuoka, Japan). For live cell video microscopy, the system *was* maintained at 37°C with 5% CO2 throughout the experiment. Image analysis was done using *I*mage-Pro Plus 10 (Media Cybernetics, Inc., Rockville, Maryland, USA) to quantify the time it takes for the gap to close to the 50% of its original area.

Trichrome/H&E staining and quantification

After paraffin processing, embedding and sectioning of the formalin fixed lung tissue, lung sections were stained with Hematoxylin and Eosin (H&E) and Masson's Trichrome dyes. Leica Aperio AT2 slide scanner (Leica Microsystems, GmbH, Wetzlar, Germany) was used to scan whole slides at 20X magnification to get a resolution of 0.5micron/pixel. The images were converted to tiff files using Aperio ImageScope software. Tumor areas in WT and GsdmD$^{-/-}$ mice were manually chosen and quantified on H&E stained slides using Image-Pro Plus 10 (Media Cybernetics, Inc., Rockville, Maryland, USA). Percent tumor area was calculated as followed: Percent tumor area = (Total tumor area ÷ Total tissue area)×100. Collagen content in WT and GsdmD was quantified on Trichrome stained slides using Image-Pro Plus 10 (Media Cybernetics, Inc., Rockville, Maryland, USA).

Mac-3 staining for macrophage infiltration

Lung tissue sections were deparaffinized using serial washes with xylenes and ethanol, followed by antigen retrieval using the Antigen-unmasking solution (Vector Labs #H-3301). Samples were washed with water, quenched for endogenous peroxidase activity using Bloxall (Vector Labs #SP-6000), followed by blocking with 5% BSA in PBS overnight in a humidified chamber at 4C. Samples were then probed with CD107b/Mac3 (BD biosciences #550292) antibody at 1:200 dilution for 1h in animal free blocker and diluent (Vector Labs #SP-5035). Sections were then washed with 0.05% Tween 20 in PBS., and subjected to Vector lab VECTASTAIN Elite ABC-HRP Kit (#PK-6104) followed by development using the Vector NovaRED kit (Vector Labs #SK-4800) both according to manufacturer instructions. Tissue sections were counterstained using hematoxylin (Vector Labs #H-3401) according to manufacturer instructions, mounted and imaged at 4x and 40x under brightfield microscopy.

Western blotting

The excised tumors were weighed and equal size tissue was homogenized in tissue lysis buffer (TPER, Thermo Scientific, 78510) supplemented with EDTA free protease inhibitor cocktail (Thermo Scientific, 87785), with ratio of ~0.1g of tissue to 1 mL T-PER lysis buffer. The cell debris was separated by centrifugation at 10,000g for 10 min. After discarding the pellet, the protein concentration was determined using

the BCA protein assay (Pierce). 10–50 μg of cell protein samples were resolved on Novex 4–20% Tris-Glycine Gels (Invitrogen) and transferred onto polyvinylidene fluoride membranes (Invitrogen). Blots were incubated with 1:1000 rabbit polyclonal antibody against cleaved IL-1β (Cell Signaling #63124), cleaved GsdmD (Cell Signaling #50928), or β-actin (Cell Signaling #8457 for 4h at RT or for 16 h at 4°C. The membranes were washed with PBST for 5 min × 3 times and incubated with 1:15000 horseradish peroxidase-conjugated goat anti-rabbit secondary antibody (Biorad) for 2h. The signal was detected with an enhanced chemiluminescent substrate (Pierce) and membranes were imaged using iBright CL750 Imaging System (Life Technologies, A44116). The western blot bands were quantified via densitometry using the iBright Analysis Software.

qRT-PCR assays

Total RNA was isolated from the cell pellets using RNeasy Mini Kit (Qiagen Inc. Valencia, CA). One μg of total RNA was reverse transcribed using the iScript cDNA kit (Biorad). Primers were purchased from ThermoFisher; AIM2 (Mm01295719), NLRP3 (Mm00840904), and beta-actin (Mm02619580). Real-time PCR amplification was performed using TaqMan and gene-specific primers in a QuantStudio 3 Real-Time PCR System (Applied Biosystems). The relative amount of target mRNA was determined using the cycle threshold (Ct) method by normalizing target mRNA Ct values to that of β-actin. The Fold induction ratios were calculated relative to control sample for each group using the formula $2^{-\Delta\Delta Ct}$.

Generation of myeloid-specific KO of GsdmD in mice

To isolate bone marrow, donor mice (female, 6–12 weeks of age) were sacrificed by CO2 asphyxiation followed by cervical dislocation. Femurs and tibias were dissected free of tissue and flushed with sterile PBS. Each mice yields approximately 4×10^7 cells, thus each donor can provide bone marrow for ~3 recipients. Bone marrow cells were centrifuged and suspended in sterile PBS prior to injection.

Recipient mice: 5-week-old female or male mice were lethally irradiated (600RAD 2x from the cesium source of the Shepard Irradiator). Four hours later, mice received $\sim 10^7$ bone marrow cells in 200 μL sterile PBS by intravenous injection into the tail vein. Mice were monitored daily for signs of sepsis (lack of eating, drinking, socializing, grooming, hunched posture, shivering, lethargy). Four weeks after irradiation, mice were treated with a single dose of liposomal clodronate to deplete sessile Kupffer cells that are radio-resistant. Kupffer cells are replenished within 7 days after clodronate. Clodronate containing liposomes were diluted in sterile saline and injected in a 0.20 mL volume of a 1 mg/mL solution and Clodronate was given via tail vein injection.

Quantification and statistical analysis

Comparisons of 2 groups were performed by a 2-tailed t test, and comparisons of 3 or more groups were performed by ANOVA with Bonferroni posttest. All statistics were performed using Prism software (GraphPad). For survival studies, the log rank test, non-parametric test, was used.